Eur. Phys. J. C 49, 675–684 (2007)
DOI 10.1140/epjc/s10052-006-0146-x

THE EUROPEAN PHYSICAL JOURNAL C

Regular Article – Theoretical Physics

Dipole model for double meson production in two-photon interactions at high energies

V.P. Gonçalves[1], M.V.T. Machado[2,a]

[1] Instituto de Física e Matemática, Universidade Federal de Pelotas, Caixa Postal 354, CEP 96010-090, Pelotas, RS, Brazil
[2] Universidade Federal do Pampa, Centro de Ciências Exatas e Tecnológicas, Campus de Bagé, CEP 96412-420, Bagé, RS, Brazil

Received: 30 May 2006 / Revised version: 11 September 2006 /
Published online: 2 December 2006 –

Abstract. In this work double vector meson production in two-photon interactions at high energies is investigated considering saturation physics. We extend the color dipole picture for this process and study the energy and virtuality dependence of the forward differential cross section. A comparison with previous results is presented, and the contribution of the different photon polarizations is estimated.

1 Introduction

The high energy limit of perturbative QCD is characterized by a center-of-mass energy which is much larger than the hard scales present in the problem. In this regime the parton densities inside the projectiles grow as energy increases, leading to the rise of the cross sections. As long the energy is not too high, we have low values of the partonic density, and the QCD dynamics is described by linear (BFKL/DGLAP) evolution equations [1–6]. However, at higher energies the parton density increases and the scattering amplitude tends to the unitarity limit. Thus, a linear description breaks down, and one enters the saturation regime, where the dynamics is described by a nonlinear evolution equation and the parton densities saturate [7–18]. The transition line between the linear and nonlinear regimes is characterized by the saturation scale $Q_{\rm sat}(x)$, which is energy dependent and sets the critical transverse size for the unitarization of the cross sections. In other words, unitarity is restored by including nonlinear corrections in the evolution equations. Such effects are small for $k_\perp^2 > Q_{\rm sat}^2$ and very strong for $k_\perp^2 < Q_{\rm sat}^2$, leading to saturation of the scattering amplitude, where $k_\perp$ is the typical hard scale present in the process. The successful description of all inclusive and diffractive deep inelastic data at the collider HERA by saturation models [19–23] suggests that these effects might become important in the energy regime probed by current colliders. Furthermore, the saturation model was extended to two-photon interactions at high energies in [24], also providing a very good description of the data on the $\gamma\gamma$ total cross section, on the photon structure function at low x and on the $\gamma^*\gamma^*$ cross section. The formalism used in [24] is based on the dipole picture [25–28], with the $\gamma^*\gamma^*$ total cross sections being described by the interaction of two color dipoles, which the virtual photons fluctuate into (for a previous analysis using the dipole picture see, e.g., [29–32]). The dipole–dipole cross section is modeled considering the saturation physics. The successful descriptions of the $\gamma\gamma$ interactions and light/heavy vector meson production for ep collisions at HERA are our main motivations to extend this formalism to describe double meson production and analyze the effects of the saturation physics.

In the last few years double meson production has been studied considering different approaches and approximations for the QCD dynamics [32–41]. In particular, in our previous paper in [36], we have performed a phenomenological analysis for double J/Ψ production using the forward LLA BFKL solution. In that case, the hard scale was set by the charm quark mass. There, we also studied the possible effects of corrections at next to leading approximation (NLA) level to the BFKL kernel investigating the influence of a smaller effective hard pomeron intercept. Afterwards, in [38] the non-forward solution was considered for a larger set of possible vector meson pairs, where the large t values provide the perturbative scale. Moreover, in that paper double vector meson production in real photon interactions was studied, the t-dependence of the differential cross section was analyzed in detail, and the total cross section for different combinations of vector mesons was calculated using the leading order impact factors and BFKL amplitude. More recently, two other studies on the process $\gamma^*\gamma^* \to VV$ have appeared in the literature [40, 41]. In the first one [40], the leading order BFKL amplitude for exclusive diffractive two-ϱ production in the forward direction is computed and the NLA corrections are estimated using a specific resummation of higher order effects. In the latter paper [41], the amplitude for forward electroproduction of two light vector mesons in NLA is computed. In particu-

[a] e-mail: magnus@if.ufrgs.br

lar, the NLA amplitude is constructed by the convolution of the $\gamma^* \to V$ impact factor and the BFKL Green's function in the $\overline{MS}$ scheme. In addition, a procedure to get results independent from the energy and renormalization scales has been investigated within the NLA approximation. A shortcoming of those approaches is that they consider only the linear regime of the QCD dynamics, and nonlinear effects associated to the saturation physics are disregarded. However, double meson production in two-photon interactions at high energies offers an ideal opportunity for studying the transition between the linear and saturation regimes, since virtualities of both photons in the initial state can vary as well as the vector mesons in the final state. In the interaction of two highly virtual photons and/or double heavy vector meson production we expect the dominance of hard physics (linear regime). In the opposite case, characterized by double light vector meson production on real photons scattering, the soft physics is expected to be dominant. Consequently, for an intermediate scenario we may expect that the main contribution comes from semi-hard physics, determined by saturation effects.

In this paper we derive the main formulas to describe double meson production in the dipole picture and analyze double meson production in two-photon interactions. We consider three cases of physical and phenomenological interest: (a) the interaction of real photons, and the interaction of virtual photons with (b) equal and (c) different virtualities.

In all cases we calculate the forward differential cross section for $\varrho\varrho$, $\varrho J/\Psi$ and $J/\Psi J/\Psi$ production. Moreover, we present a comparison between the linear and nonlinear predictions and estimate the contribution for distinct photon polarizations.

2 Basic formulas

2.1 Double meson production in the dipole picture

Let us introduce the main formulas concerning vector meson production in the color dipole picture. First, we consider the scattering process $\gamma\gamma \to V_1\, V_2$, where V_i stands for both light and heavy mesons. At high energies, the scattering process can be seen as a succession in time of three factorizable subprocesses: i) the photon fluctuates in quark–antiquark pairs (the dipoles), ii) these color dipoles interact and, iii) the pairs convert into the vector mesons final states.

Using as kinematic variables the $\gamma^*\gamma^*$ c.m.s. energy squared $s = W^2 = (p+q)^2$, where p and q are the photon momenta, the photon virtualities squared are given by $Q_1^2 = -q^2$ and $Q_2^2 = -p^2$. The x_{12} variable is defined by

$$x_{12} = \frac{Q_1^2 + Q_2^2 + M_{V_1}^2 + M_{V_2}^2}{W^2 + Q_1^2 + Q_2^2}\,. \tag{1}$$

The corresponding imaginary part of the amplitude at zero momentum transfer reads

$$\begin{aligned}
&\mathrm{Im}\,\mathcal{A}(\gamma^*\gamma^* \to V_1 V_2) \\
&= \sum_{h,\bar{h}} \sum_{n,\bar{n}} \int \mathrm{d}z_1\, \mathrm{d}^2 r_1 \Psi^{\gamma}_{h,\bar{h}}\big(z, r_1, Q_1^2\big) \Psi^{V_1 *}_{h,\bar{h}}(z_1, r_1) \\
&\quad \times \int \mathrm{d}z_2\, \mathrm{d}^2 r_2 \Psi^{\gamma}_{n,\bar{n}}\big(z_2, r_2, Q_2^2\big) \Psi^{V_2 *}_{n,\bar{n}}(z_2, r_2) \sigma_{dd}(x_{12}, r_1, r_2)\,,
\end{aligned} \tag{2}$$

where Ψ^{γ} and Ψ^{V_i} are the light-cone wavefunctions of the photon and vector meson, respectively. The quark and antiquark helicities are labeled by h, $\bar{h}$, n and $\bar{n}$ and reference to the meson and photon helicities is implicitly understood. The variable r_1 defines the relative transverse separation of the pair (dipole) and z_1 $(1 - z_1)$ is the longitudinal momentum fractions of the quark (antiquark). Similar definitions are valid for r_2 and z_2. The basic blocks are the photon wavefunction, Ψ^{γ}, the meson wavefunction, $\Psi^{V}_{\mathrm{T,L}}$, and the dipole–dipole cross section, σ_{dd}.

In the dipole formalism, the light-cone wavefunctions $\Psi_{h,\bar{h}}(z, r)$ in the mixed representation (r, z) are obtained through the two dimensional Fourier transform of the momentum space light-cone wavefunctions $\Psi_{h,\bar{h}}(z, \mathbf{k})$ (see for more details, e.g., [42–44]). The normalized light-cone wavefunctions for longitudinally (L) and transversely (T) polarized photons are given by

$$\Psi^{\mathrm{L}}_{h,\bar{h}}(z, r) = \sqrt{\frac{N_{\mathrm{c}}}{4\pi}}\, \delta_{h,-\bar{h}}\, e e_f\, 2z(1-z) Q \frac{K_0(\varepsilon r)}{2\pi}\,, \tag{3}$$

$$\begin{aligned}
\Psi^{\mathrm{T}(\gamma=\pm)}_{h,\bar{h}}(z, r) = \pm \sqrt{\frac{N_{\mathrm{c}}}{2\pi}}\, e e_f \big[&\mathrm{i} \mathrm{e}^{\pm \mathrm{i}\theta_r} (z \delta_{h\pm,\bar{h}\mp} \\
&- (1-z)\delta_{h\mp,\bar{h}\pm}) \partial_r + m_f \delta_{h\pm,\bar{h}\pm} \big] \frac{K_0(\varepsilon r)}{2\pi}\,,
\end{aligned} \tag{4}$$

where $\varepsilon^2 = z(1-z)Q^2 + m_f^2$. The quark mass m_f plays the role of a regulator when the photoproduction regime is reached. Namely, it prevents a non-zero argument for the modified Bessel functions $K_{0,1}(\varepsilon r)$ towards $Q^2 \to 0$. The electric charge of the quark of flavor f is given by $e e_f$.

For vector mesons, the light-cone wavefunctions are not known in a systematic way and should be modeled. The simplest approach assumes the same vector current as in the photon case, but introducing an additional vertex factor. Moreover, in general the same functional form is chosen for the scalar part of the meson light-cone wavefunction. Here, we follow the analytically simple DGKP approach [45]. In this particular approach, one assumes that the dependences on r and z of the wavefunction are factorized, with a Gaussian dependence on r. Its main shortcoming is that it breaks the rotational invariance between transverse and longitudinally polarized vector mesons [46, 47]. However, as it describes reasonably the HERA data for vector meson production, as pointed out in [44, 48], we will use it in our phenomenological analysis. The DGKP longitudinal and transverse meson light-cone wavefunctions are given by [45]

Table 1. Parameters and normalization of the DGKP vector meson light-cone wavefunctions. The results have been obtained using quark mass values from the saturation model (see text)

V (m_V) [MeV]	$\hat{e}_V$	f_V [GeV]	$\omega_{\rm T}$ [GeV]	$\mathcal{N}_{\rm T}$	$\omega_{\rm L}$ [GeV]	$\mathcal{N}_{\rm L}$
ϱ (770)	$1/\sqrt{2}$	0.153	0.218	8.682	0.331	15.091
J/Ψ (3097)	2/3	0.270	0.546	7.665	0.680	19.350

$$\Psi^{V,{\rm L}}_{h,\bar{h}}(z,r) = z(1-z)\delta_{h,-\bar{h}}\frac{\sqrt{\pi}f_V}{2\sqrt{N_{\rm c}}\hat{e}_f} f_{\rm L}(z)\exp\left[\frac{-\omega_{\rm L}^2 r^2}{2}\right], \tag{5}$$

$$\begin{aligned}\Psi^{V,{\rm T}(\gamma=\pm)}_{h,\bar{h}}&(z,r)\\ &= \pm\left(\frac{{\rm i}\omega_{\rm T}^2 r {\rm e}^{\pm {\rm i}\theta_r}}{m_V}[z\delta_{h\pm,\bar{h}\mp} - (1-z)\delta_{h\mp,\bar{h}\pm}] + \frac{m_f}{m_V}\delta_{h\pm,\bar{h}\pm}\right)\\ &\quad\times\frac{\sqrt{\pi}f_V}{\sqrt{2N_{\rm c}}\hat{e}_f} f_{\rm T}(z)\exp\left[\frac{-\omega_{\rm L}^2 r^2}{2}\right],\end{aligned} \tag{6}$$

where $\hat{e}_f$ is the effective charge arising from the sum over quark flavors in the meson of mass m_V. The following values stand for the ϱ and J/Ψ mesons, respectively: $\hat{e}_f = 1/\sqrt{2}$ and $2/3$. The coupling of the meson to the electromagnetic current is labeled by $f_V^2 = 3m_V\Gamma_{e^+e^-}/4\pi\alpha_{\rm em}^2$ (see Table 1). The function $f_{\rm T,L}(z)$ is given by the Bauer–Stech–Wirbel model [49]:

$$f_{\rm T,L}(z) = \mathcal{N}_{\rm T,L}\sqrt{z(1-z)}\exp\left[\frac{-m_V^2(z-1/2)^2}{2\omega_{\rm T,L}^2}\right]. \tag{7}$$

The meson wavefunctions are constrained by the normalization condition, which contains the hypothesis that the meson is composed only of quark–antiquark pairs, and by the electronic decay width $\Gamma_{V\to e^+e^-}$. Both conditions are respectively given by [43, 50]

$$\sum_{h,\bar{h}}\int {\rm d}^2r\,{\rm d}z\left|\Psi^{V(\lambda)}_{h,\bar{h}}(z,r)\right|^2 = 1\,, \tag{8}$$

$$\begin{aligned}\sum_{h,\bar{h}}\int\frac{{\rm d}^2r}{(2\pi)^2}&\frac{{\rm d}z}{z(1-z)}\left[z(1-z)Q^2 + k^2 + m_f^2\right]\\ &\times\Psi^V_{h,\bar{h}}(k,z)\Psi^{\gamma^*}_{h,\bar{h}}(k,z) = ef_V m_V\left(\varepsilon^*_\gamma\varepsilon_V\right).\end{aligned} \tag{9}$$

The constraints above, when used on the DGKP wavefunction, imply the following relations [44]:

$$\omega_{\rm L,T} = \frac{\pi f_V}{\sqrt{2N_{\rm c}}\hat{e}_f}\sqrt{I_{\rm L,T}}\,, \tag{10}$$

$$\begin{aligned}\int_0^1 {\rm d}z z(1-z)f_{\rm L}(z) &= \int_0^1 {\rm d}z\frac{2[z^2+(1-z)^2]\omega_{\rm T}^2 + m_f^2}{2m_V^2 z(1-z)}f_{\rm T}(z)\\ &= 1\,,\end{aligned} \tag{11}$$

where

$$I_{\rm L} = \int_0^1 {\rm d}z z^2(1-z)^2 f_{\rm L}^2(z), \tag{12}$$

$$I_{\rm T} = \int_0^1 {\rm d}z\frac{[z^2+(1-z)^2]\omega_{\rm T}^2 + m_f^2}{m_V^2}f_{\rm T}^2(z)\,. \tag{13}$$

The relations in (10) come from the normalization condition, whereas the relations in (11) are a consequence of the leptonic decay width constraints. The parameters $\omega_{\rm T,L}$ and $\mathcal{N}_{\rm T,L}$ are determined by solving (10) and (11) simultaneously. In Table 1 we quote the results which will be used in our further analysis. To be consistent with the saturation models, which we will discuss further, we have used the quark masses $m_{u,d,s} = 0.14$ GeV and $m_c = 1.5$ GeV. We quote [44, 48] for more details in the present approach and its comparison with data for both photo- and electroproduction of vector mesons.

Finally, the imaginary part of the forward amplitude can be obtained by putting the expressions for photon and vector meson (DGKP) wavefunctions, (3)–(6), into (2). Moreover, summation over the quark/antiquark helicities and an average over the transverse polarization states of the photon should be taken into account. In order to obtain the total cross section, we assume an exponential parameterization for the small $|t|$ behavior of the amplitude. After integration over $|t|$, the total cross section for double vector meson production by real/virtual photons reads

$$\begin{aligned}\sigma(\gamma\gamma\to V_1V_2) &= \frac{1}{B_{V_1V_2}}\left.\frac{{\rm d}\sigma(\gamma\gamma\to V_1V_2)}{{\rm d}t}\right|_{t_{\rm min}=0}\\ &= \frac{[{\rm Im}\,\mathcal{A}(s,t=0)]^2}{16\pi B_{V_1V_2}}(1+\beta^2)\,,\end{aligned} \tag{14}$$

where β is the ratio of real to imaginary part of the amplitude and $B_{V_1V_2}$ is the slope parameter.

2.2 Dipole–dipole cross section in the saturation model

The dipole formulation has been extensively used in the description of inclusive and diffractive processes at HERA in an unified way. The basic quantity is the dipole–proton cross section $\sigma_{\rm dip}$, which contains all information about the target and the strong interaction physics. In general, the saturation models [19–23] interpolate between the small and large dipole configurations, providing color transparency behavior, $\sigma_{\rm dip}\sim r^2$, at $r \ll 1/Q_{\rm sat}$,and constant behavior at large dipole separations, $r > 1/Q_{\rm sat}$. The

physical scale which characterizes the transition between the dilute and saturated system is denoted the saturation scale, $Q^2_{\rm sat} \propto x^{-\lambda}$, which is energy dependent. Along these lines, the phenomenological saturation model proposed by Golec-Biernat and Wüsthoff (GBW) [19, 20] resembles the main features of the Glauber–Mueller resummation. Namely, the dipole cross section in the GBW model takes the eikonal-like form,

$$\sigma_{\rm dip}^{\rm GBW}(x,r) = \sigma_0 \left[1 - \exp\left(- \frac{Q^2_{\rm sat}(x) r^2}{4} \right) \right]. \qquad (15)$$

Its phenomenological application has been successful in a wide class of processes with a photon probe. Although the GBW model describes reasonably well the HERA data, its functional form is only an approximation of the theoretical nonlinear QCD approaches [7–18]. The parameters of the model are $\sigma_0 = 29.12\,{\rm mb}$, the masses of the light quarks (u, d, s) $m_f = 0.14\,{\rm GeV}$, and the charm mass $m_c = 1.5\,{\rm GeV}$. Moreover, the saturation scale is given by $Q_{\rm sat} = (x_0/x)^{\lambda/2}$, with the parameters $x_0 = 4.1 \times 10^{-5}$ and $\lambda = 0.277$. In [23] a parameterization for the dipole cross section was constructed to smoothly interpolate between the limiting behaviors analytically under control: the solution of the BFKL equation for small dipole sizes, $r \ll 1/Q_{\rm sat}(x)$, and the Levin–Tuchin law [51] for larger ones, $r \gg 1/Q_{\rm sat}(x)$. A fit to the structure function $F_2(x, Q^2)$ was performed in the kinematical range of interest, showing that it is not very sensitive to the details of the interpolation. The dipole cross section was parameterized as follows:

$$\sigma_{\rm dip}^{\rm IIM}(x,r) = \sigma_0 \begin{cases} \mathcal{N}_0 \left(\dfrac{r Q_{\rm sat}}{2} \right)^{2\left(\gamma_{\rm sat} + \frac{\ln(2/rQ_{\rm sat})}{\kappa \lambda Y}\right)}, \\ \qquad\qquad \text{for } r Q_{\rm sat}(x) \leq 2\,, \\ 1 - \exp\left[- a \ln^2 (b r Q_{\rm sat}) \right], \\ \qquad\qquad \text{for } r Q_{\rm sat}(x) > 2\,, \end{cases} \qquad (16)$$

where the expression for $r Q_{\rm sat}(x) > 2$ (saturation region) has the correct functional form, as obtained either by solving the Balitsky–Kovchegov (BK) equation [7–9], or from the theory of the color glass condensate (CGC) [10–18]. Hereafter, we label the model above by IIM. The coefficients $a = 1.8$ and $b = 1.13$ are determined from the continuity conditions of the dipole cross section at $r Q_{\rm sat}(x) = 2$. The coefficients $\gamma_{\rm sat} = 0.63$ and $\kappa = 9.9$ are fixed from their LO BFKL values. In our further calculations will be used the parameters $R_{\rm p} = 0.641\,{\rm fm}$, $\lambda = 0.253$, $x_0 = 0.267 \times 10^{-4}$ and $\mathcal{N}_0 = 0.7$, which give the best fit result. It is important to emphasize that the GBW and IIM saturation models are suitable in the region below $x = 0.01$ and the large x limit needs still a consistent treatment. At ep collisions the dipole–proton cross sections should be supplemented by a threshold factor $(1-x)^{n_{\rm thres}}$, with $n_{\rm thres} = 5$, which is directly associated with the number of spectators at $x \approx 1$ ($n_{\rm thres} = 2 n_{\rm spect} - 1$).

Following [24] we can extend the saturation model, originally proposed to describe ep collisions, to two-photon interactions at high energies. The basic idea is that the dipole–dipole cross section $\sigma_{dd}(x_{12}, r_1, r_2)$ has the same functional form as the dipole–proton one and is expressed in terms of an effective radius $r_{\rm eff}$, which depends on r_1 and/or r_2. Consequently, we have [24]

$$\sigma_{dd}^{\rm GBW}(x_{12}, r_{\rm eff}) = \hat{\sigma}_0 \left[1 - \exp\left(- \frac{Q^2_{\rm sat}(x_{12}) r^2_{\rm eff}}{4} \right) \right], \qquad (17)$$

and

$$\sigma_{\rm dip}^{\rm IIM}(x_{12}, r_{\rm eff}) = \sigma_0 \begin{cases} \mathcal{N}_0 \left(\dfrac{r_{\rm eff} Q_{\rm sat}}{2} \right)^{2\left(\gamma_{\rm sat} + \frac{\ln(2/r_{\rm eff}Q_{\rm sat})}{\kappa \lambda Y}\right)}, \\ \qquad\qquad \text{for } r_{\rm eff} Q_{\rm sat}(x_{12}) \leq 2\,, \\ 1 - \exp\left[- a \ln^2 (b r_{\rm eff} Q_{\rm sat}) \right], \\ \qquad\qquad \text{for } r_{\rm eff} Q_{\rm sat}(x_{12}) > 2\,, \end{cases} \qquad (18)$$

where the x_{12} variable is given by (1) and $\hat{\sigma}_0 = \frac{2}{3}\sigma_0$, with σ_0 the same as in [19, 20, 23] and referred to above. The last relation can be justified in terms of the quark counting rule. In the two-photon case, the resulting quark masses are slightly different as it was found in [24]: $m_f = 0.21\,{\rm GeV}$ for the light quarks and $m_c = 1.3\,{\rm GeV}$ for the charm quark. In [24] three different scenarios for $r_{\rm eff}$ have been considered, with the dipole–dipole cross section presenting in all cases the color transparency property ($\sigma_{dd} \to 0$ for $r_1 \to 0$ or $r_2 \to 0$) and saturation ($\sigma_{dd} \to \hat{\sigma}_0$) for large size dipoles. We quote also [52] for interesting discussions on the effective radius and its consequences in hadron–hadron interactions. In what follows, we use model I from [24], where $r^2_{\rm eff} = r_1^2 r_2^2/(r_1^2 + r_2^2)$, which is favored by the $\gamma^*\gamma^*$ and F_2^γ data. We have tested the sensitivity of the result to a different prescription, $r^2_{\rm eff} = \min(r_1^2, r_2^2)$ (named model II in [24]). Its deviation from model I is quite large for ϱ production and almost insensitive for mixed $\varrho J/\Psi$ production. For double J/Ψ production the deviation is considerably larger than the mixed one. However, the difference concerns only the overall normalization, and no change is seen in the energy behavior. Moreover, in order to extend the dipole model to large x_{12}, it is necessary to take into account threshold correction factors which constrain the cross section to vanish when $x_{12} \to 1$ as a power of $1 - x_{12}$. As in [24], we multiply the dipole–dipole cross section by the factor $(1 - x_{12})^5$.

A comment is in order here. One shortcoming of the GBW model is that it does not contain the correct DGLAP limit at large virtualities. Consequently, we may expect that its predictions are only valid at small values of the photon virtualities. Therefore, in what follows we only consider photon virtualities up to $10\,{\rm GeV}^2$.

In Fig. 1a we present the dependence of the two dipole–dipole cross sections, (17) and (18), as a function of the effective radius $r_{\rm eff}$ at different values of x_{12} ($x_{12} = 10^{-n}$, $n = 1, 2, 3, 4$). We see that at small values of $r_{\rm eff}$ their predictions are similar, while they differ approximately 15% at large $r_{\rm eff}$ and small values of x_{12}. In order to emphasize the importance of the saturation effects, in Fig. 1b we present a comparison between the full predictions of the

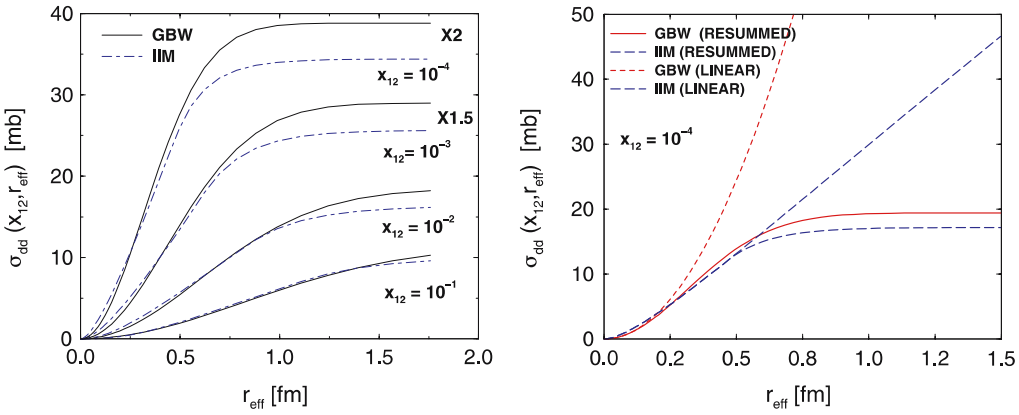

Fig. 1. Dipole–dipole cross sections: **a** comparison between the predictions for the GBW and IIM models at different values of x_{12}; **b** comparison between their resummed predictions and the corresponding linear limits

GBW and IIM dipole–dipole cross sections and their linear limits. We have denoted by 'resummed' the curves with the complete expressions in (17) and (18) and by 'linear' their approximations in the limit of small dipoles. Namely, for the linear case one has $\sigma_{dd}^{\rm GBW} \propto \hat{\sigma}_0(Q_{\rm sat}^2 r_{\rm eff}^2/4)$ and for the IIM model we just take the extrapolation of (18) for $r_{\rm eff} \leq 2/Q_{\rm sat}$. We see that at $r_{\rm eff} \approx 0.2\,$fm the linear and resummed predictions from the GBW model start to be different. On the other hand, in the IIM case, this difference starts at $r_{\rm eff} \approx 0.5\,$fm. Consequently, the transition between the linear and saturation regimes is distinct in the GBW and IIM models.

In the next section we will compare the predictions for double meson production coming from different models for the dipole–dipole cross section. However, the extension of the IIM model for photon–photon interactions has not been considered before. For the sake of completeness, we compare the predictions of the GBW and IIM models for the specific cases of the total $\gamma\gamma$ cross section and heavy quark production. The analysis of heavy quark production is motivated by its strict relation with double J/Ψ production. The GBW model has already been considered in [24], while the IIM analysis is the first one in the literature. In Fig. 2a we present a comparison between the predictions of the GBW and IIM models for the total cross section and the OPAL and L3 experimental data [53, 54]. Following [24] we also include the QPM and reggeon contribution and assume model I for the effective radius. We have that the GBW and IIM predictions are similar, describing the current experimental data quite well. It should be noticed that the parameters for IIM have not been adjusted in order to fit the two-photon data as done for GBW. Furthermore, we compute the cross section for charm production in the reaction $\gamma\gamma \to c\bar{c}$, considering real photons. The results are presented in Fig. 2b for two prescriptions of the effective radius (model I and II as referred to before) and are compared with the L3 data. The low energy quark box contribution (QPM) has been added. An additional contribution, which we do not include, is the resolved (single and double) piece to the charm cross section, which reaches 30% of the main contribution at high energies. As already verified in [24], both prescriptions for the effective radius provide a reasonable description of the data when the GBW model is considered. On the other hand, in the IIM model, prescription I for the effective radius gives a better description, with model II overestimating the L3 data at high energies. Moreover, the IIM model implies a stronger energy dependence of the heavy quark production cross section than the GBW prediction. This behavior should also be present in other processes characterized by a hard scale as, for instance, the interaction of two highly virtual photons or double heavy vector meson production.

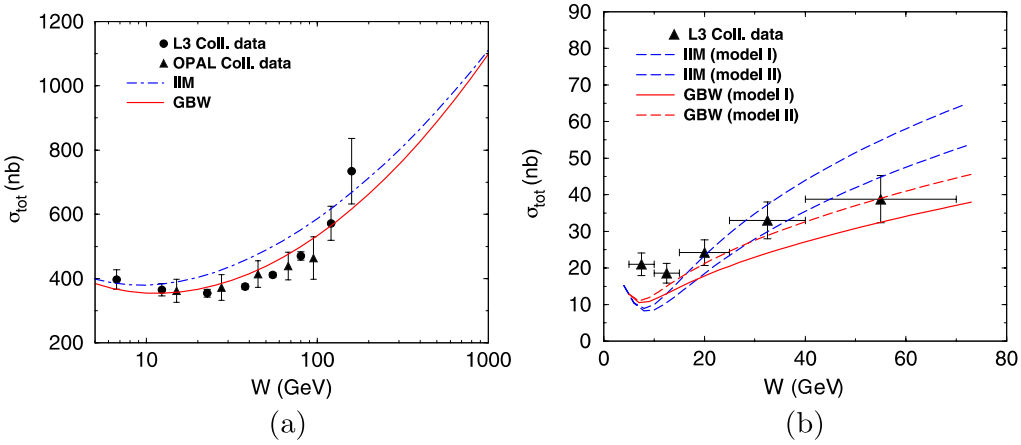

Fig. 2. A comparison between the predictions for **a** the total cross section and **b** charm production in two real photon collisions considering the GBW and IIM dipole–dipole cross sections. The QPM contribution has been added. The data from the OPAL and L3 Collaborations

In what follows we only will consider model I for the effective radius.

3 Results

In order to calculate the total cross section for double vector meson production given in (14) it is necessary to specify the value of the slope parameter $B_{V_1V_2}$. As this quantity is not well constrained, in what follows we only will present our predictions for the energy and virtuality dependence of the forward differential cross section $\frac{\mathrm{d}\sigma(\gamma\gamma\to V_1V_2)}{\mathrm{d}t}\Big|_{t_{\rm min}=0}$. This should be enough for the present level of accuracy. We start by the study of the scattering of two real photons, investigating its dependence on energy and on the mesons mass. Afterwards, we consider the scattering of virtual photons and investigate the symmetric ($Q_1^2 = Q_2^2$) and asymmetric ($Q_1^2 \propto \alpha Q_2^2$ with $\alpha \gg 1$) cases. In addition, we estimate the magnitude of the contribution of the distinct polarizations for the total cross sections. Finally, we discuss the size of parton saturation effects in the production of different mesons.

3.1 Double meson production on real photons interactions

Let us start our analyses considering double meson production in two real photon scattering. In Fig. 3 we present the forward differential cross sections for the representative cases of double ϱ, $\varrho J/\Psi$ and double J/Ψ production in the energy range $50\,\mathrm{GeV} \leq W_{\gamma\gamma} \leq 10^3\,\mathrm{GeV}$. The curves are presented for the two models of the dipole–dipole cross section given in (17) and (18). Bold curves stand for the GBW model and thin curves for the IIM model. The forward differential cross section is sizeable in the double ϱ case, being of order 20–40 nb/GeV^2 in the energy range considered. Mixed $\varrho J/\Psi$ production is the second higher rate, reaching 4–40 pb/GeV^2, whereas double J/Ψ production is quite low. The deviations between the GBW and IIM models are large for double ϱ production, with the IIM results being a factor 10 below the GBW ones at $W_{\gamma\gamma} \approx 1$ TeV. The origin of this discrepancy is not clear, since there is no evidence for strong deviations in the $\gamma\gamma$ case shown in Fig. 2a. Probably, deviations could come from the different weights given by the wavefunctions in each case. This subject requires further investigation. For double J/Ψ production, the IIM prediction overestimates the GBW one by a factor 4, which agrees with the expectation which comes from our previous results for heavy quark production (see Fig. 2b). On the other hand, in the $\varrho J/\Psi$ case, the results are equivalent at low energies but differ by a factor 2 at 1 TeV, with the GBW prediction being greater than the IIM. These features can be qualitatively understood in terms of the scales involved in the process. As we discussed before, the IIM dipole–dipole cross section has a relatively faster transition to saturation in comparison with GBW and underestimates it by a factor of 20–30% at small x_{12}. In double ϱ and mixed vector meson production the typical scale is given by the light meson mass $\bar{\mu}^2 = 2M_\varrho^2$ or the sum of the light–heavy meson $\bar{\mu}^2 = (M_\varrho^2 + M_{J/\Psi}^2)$. Therefore, the double ϱ process is dominated by a relatively soft scale, and saturation effects should be important, whereas mixed production is characterized by a semi-hard scale which is still sensitive to saturation effects. On the other hand, in double J/Ψ production the typical scale is sufficiently hard, $\bar{\mu}^2 = 2M_{J/\Psi}^2$. Therefore, we expect a larger contribution of small dipoles leading to a cross section with higher magnitude.

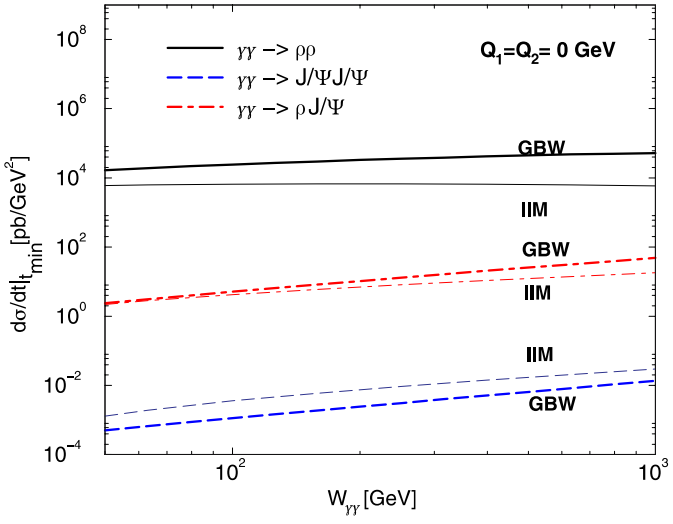

Fig. 3. Energy dependence of the forward differential cross section for double vector meson production considering real photons interactions ($Q_1^2 = Q_2^2 = 0\,\mathrm{GeV}^2$). *Bold* (*thin*) curves are the results for the GBW (IIM) parameterization for the dipole–dipole cross section

In order to analyze the energy dependence of the forward differential cross section we have performed a simple power-like fit in the energy interval $50 \leq W_{\gamma\gamma} \leq 10^3$ GeV in the form $\frac{\mathrm{d}\sigma_{V_1V_2}}{\mathrm{d}t}\Big|_{t_{\rm min}=0} \propto W_{\gamma\gamma}^{\alpha}$. For double ϱ production one obtains $\alpha = 0.4$ (0.08) for the GBW (IIM) model. In Regge phenomenology, this corresponds to an effective pomeron intercept of order $\alpha_{I\!P}^{\rm eff} \approx \alpha/4 = 0.1$ (0.02) for the GBW (IIM) parameterizations, which is clearly a soft behavior. This fact shows that the IIM model contains stronger saturation effects in contrast to the GBW one in the case of dominantly soft scales. In mixed production, the effective power increases to $\alpha = 0.96$ (0.65) for the GBW (IIM) model and the difference is not too sizeable as in the ϱ case. For double J/Ψ production, $\alpha = 1.06$ (0.9), which implies $\alpha_{I\!P}^{\rm eff} \approx 0.27$. Therefore, one has a hard pomeron behavior in the case where the heavy meson mass ($\bar{\mu}^2 = 2M_{J/\Psi}^2$) is present in the problem. Thus, as expected from the phenomenology of ep collisions, the saturation model for double vector meson production in $\gamma\gamma$ interactions is able to consistently connect the soft behavior when a non-perturbative scale is involved with the hard pomeron expectations when a perturbative scale is present.

Let us now compare our results with those obtained in other approaches [32–38]. Initially, let us consider the

previous calculations within the color dipole picture [32]. In [32] there are estimations of the total cross section for double meson production. Our predictions underestimate those results by a factor 10 for double ϱ and a factor 100 for the other mesons. In this comparison we have used the following values for the slope parameters: $B_{\varrho\varrho} = 10\,\mathrm{GeV}^{-2}$, $B_{\varrho J/\Psi} = 5\,\mathrm{GeV}^{-2}$ and $B_{J/\Psi J/\Psi} = 0.44\,\mathrm{GeV}^{-2}$, which are taken from our recent investigations on double meson production in [36, 37]. These deviations are probably due to the different dipole–dipole cross section, distinct choices for the quark masses and uncertainties in the determination of the slope parameter. For instance, the dipole–dipole cross section in [32] behaves as $\sigma_{dd} \propto r_1^4 r_2^4$ for small dipoles and $\sigma_{dd} \propto r_1^2 r_2^2$ for large dipoles, which overestimate the integration on dipole sizes in comparison with the dipole–dipole cross sections presented here. Namely, one has $\sigma_{dd} \propto r_{\rm eff}^2 Q_{\rm sat}^2$ for dipoles having transverse size $r_{\rm eff} < 1/Q_{\rm sat}$ and $\sigma_{dd} \propto \hat{\sigma}_0$ for dipoles of size $r_{\rm eff} > 1/Q_{\rm sat}$. Furthermore, $\varrho J/\Psi$ production in $\gamma\gamma$ processes has also been estimated in [35, 37]. There, the differential cross section was estimated in a way similar to elastic J/Ψ photoproduction off the proton [55]. Our results agree with these predictions, with a behavior similar to those obtained using the GRS (LO) parameterization for the gluon distribution on the ϱ meson. This process was also estimated in [38] using the non-forward solution of the BFKL equation. Our results are smaller than the estimations obtained in [38]. This is expected since the saturation effects modify significantly the cross section of this semi-hard process. Moreover, our results for double ϱ production agree with those obtained in [37] assuming the pomeron-exchange factorization. However, as its predictions are strongly dependent on the assumptions present in the calculations of double J/Ψ and $\varrho J/\Psi$ production (see Table 1 in [37]), a direct comparison is not very illuminating. This process also was analyzed in [38], but a direct comparison is not possible because only the hard contribution ($|t| > 1\,\mathrm{GeV}^2$) has been estimated.

3.2 Double meson production on virtual photons interactions

Let us now consider double vector meson production when we have the interaction of virtual photons. In Fig. 4a we present the predictions of the GBW model for the energy dependence considering that the incident photons have equal virtualities ($Q^2 = 10\,\mathrm{GeV}^2$). We have that the forward differential cross section decreases when the virtuality and/or the total mass of the final state is increased. The differential cross sections present a behavior similar on energy, independently of the meson mass. This is due to the sufficiently hard scale for these processes as given by $\mu^2 = 2Q^2 + M_{V_1}^2 + M_{V_2}^2$, which is basically determined by the high photon virtuality, since $2Q^2 \geq M_V^2$. This also explains the proximity between the $\varrho J/\Psi$ and double J/Ψ predictions, in contrast with those obtained for the real photon interactions. A power-like fit to the differential cross section in the form $\left.\frac{\mathrm{d}\sigma_{V_1V_2}}{\mathrm{d}t}\right|_{t_{\rm min}=0} \propto W_{\gamma\gamma}^{\alpha}$ gives $\alpha = 1.01, 1.08, 1.1$ for double ϱ, $\varrho J/\Psi$ and double J/Ψ, respectively. Our result for double ϱ is consistent with the NLA BFKL calculation using BLM scale fixing presented in [40].

In Fig. 4b we present our predictions for double meson production considering unequal photon virtualities. We consider the limit case of real photon scattering on a deeply virtual partner, namely $Q_1^2 = 0$ and $Q_2^2 = 10\,\mathrm{GeV}^2$. Now, the typical scale is given by $\mu^2 = Q^2 + M_{V_1}^2 + M_{V_2}^2$. In our computation of mixed production we take the following statements for the photon virtualities: Q_1^2 corresponds to the photon transforming into ϱ, and Q_2^2 corresponds to the photon transforming into J/Ψ. Notice that the final cross section should be given by $\sigma[\varrho(Q_1)J/\Psi(Q_2)$ or $\varrho(Q_2)J/\Psi(Q_1)] = \sigma[\varrho(Q_1)J/\Psi(Q_2)] + \sigma[\varrho(Q_2)J/\Psi(Q_1)]$. We see that the behavior of the different predictions are similar to those obtained in Fig. 4a, with the energy dependence for $\varrho J/\Psi$ and double J/Ψ production being almost identical to those obtained in the symmetric case. The main difference occurs for double ϱ production, which has its energy dependence strongly modified by saturation effects due to the small value of μ^2 present in the problem. A power-like fit to the differential cross section in the form $\left.\frac{\mathrm{d}\sigma_{V_1V_2}}{\mathrm{d}t}\right|_{t_{\rm min}=0} \propto W_{\gamma\gamma}^{\alpha}$ gives $\alpha = 0.65, 1.03, 1.08$ for double ϱ, $\varrho J/\Psi$ and double J/Ψ, respectively.

Using the dipole approach the contribution of the different polarizations for the forward differential cross section can be directly estimated. Let us start considering double ϱ production at equal virtualities of photons. We

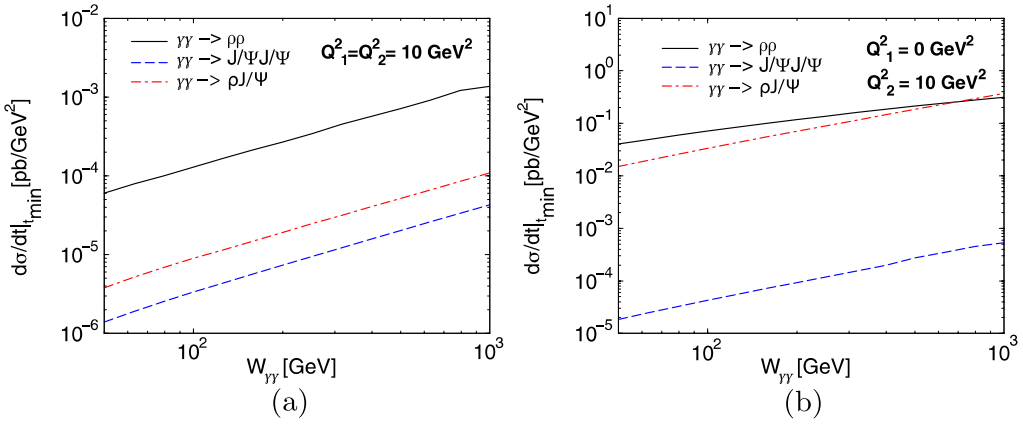

Fig. 4. Energy dependence for double vector meson production considering virtual photons considering **a** equal virtualities ($Q_1^2 = Q_2^2 = 10\,\mathrm{GeV}^2$) and **b** distinct virtualities ($Q_1^2 = 0$ and $Q_2^2 = 10\,\mathrm{GeV}^2$)

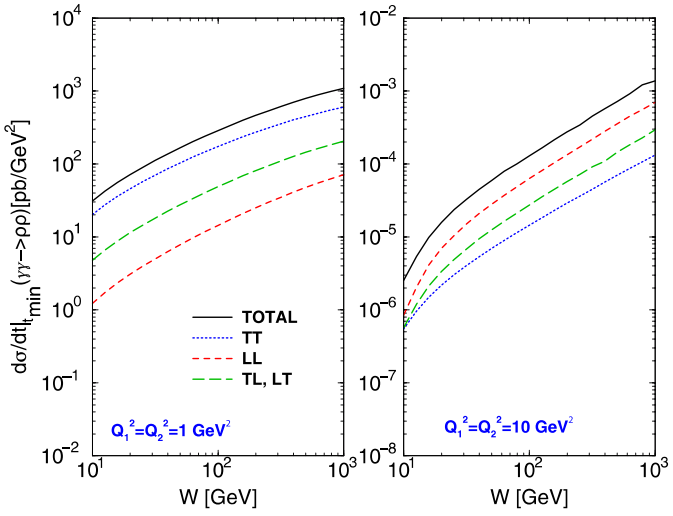

Fig. 5. Energy dependence for double ϱ production at equal photon virtualities, $Q^2 = 1$ and $Q^2 = 10\,\mathrm{GeV}^2$. The contributions of the different polarizations (TT, LL, TL/LT) are explicitly presented. See the discussion in the text

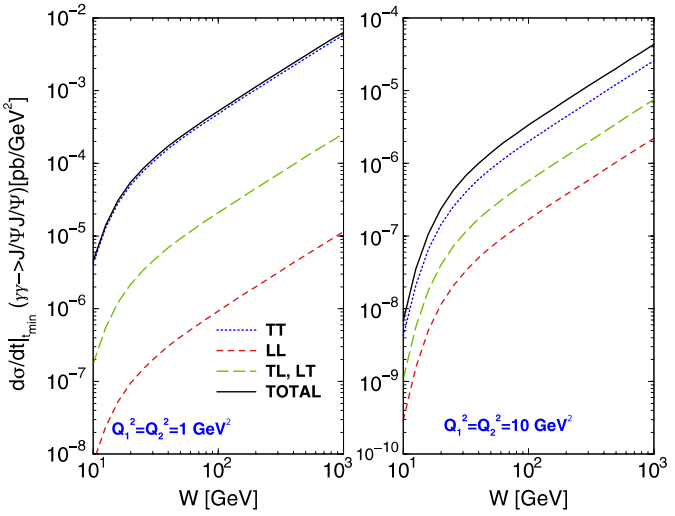

Fig. 6. Energy dependence for double J/Ψ production at equal photon virtualities, $Q^2 = 1$ and $Q^2 = 10\,\mathrm{GeV}^2$. The contributions of the different polarizations (TT, LL, TL/LT) are explicitly presented. See the discussion in the text

consider the following illustrative cases: $Q_1^2 = Q_2^2 = 1\,\mathrm{GeV}^2$ and $Q_1^2 = Q_2^2 = 10\,\mathrm{GeV}^2$. These choices allow us to observe the dependence of each contribution on virtuality. The results are shown in Fig. 5. The transverse piece (TT) is labeled by dotted curves, the longitudinal piece by dashed curves, mixed transverse–longitudinal (TL or LT) by long dashed curves and the total cross section (summation over polarizations) by solid curves. In case of production of the same vector meson, the TL and LT pieces contribute equally, TL = LT. For virtualities $Q^2 = 1\,\mathrm{GeV}^2$, the transverse content dominates, followed by the LT/LT and LL pieces. The longitudinal content is a quite small contribution, which is consistent with the longitudinal wavefunction to be proportional to the photon virtuality, which vanishes when $Q^2 \to 0$. A completely different situation occurs when the virtualities increase to $Q^2 = 10\,\mathrm{GeV}^2$. In this case the longitudinal piece is dominant, followed by the LT/LT and transverse parts. This is consistent with the ratio $\sigma_\mathrm{L}/\sigma_\mathrm{T} \geq 0$ being Q^2-dependent in light meson photoproduction (see e.g. [46, 47]).

A similar analysis can be made for double J/Ψ production (see Fig. 6). We take the same virtualities for the virtual photons and the same notation as before. For virtualities $Q_1^2 = Q_2^2 = 1\,\mathrm{GeV}^2$, the transverse content dominates, followed by the LT/LT and LL pieces. As in the double ϱ case, the longitudinal contribution is quite small. The total contribution is determined completely by the transverse contribution, with other pieces being negligible. A completely different situation occurs when the virtualities increase to $10\,\mathrm{GeV}^2$ in contrast with the ϱ case. The pattern remains the same as for $Q^2 = 1\,\mathrm{GeV}^2$, with the transverse piece still being dominant, followed by the LT/TL and LL pieces. The total contribution is slightly larger than the transverse one.

Finally, let us investigate the dependence on virtuality at fixed energy of the forward differential cross section. We take the representative energy of $W_{\gamma\gamma} = 500\,\mathrm{GeV}$. In

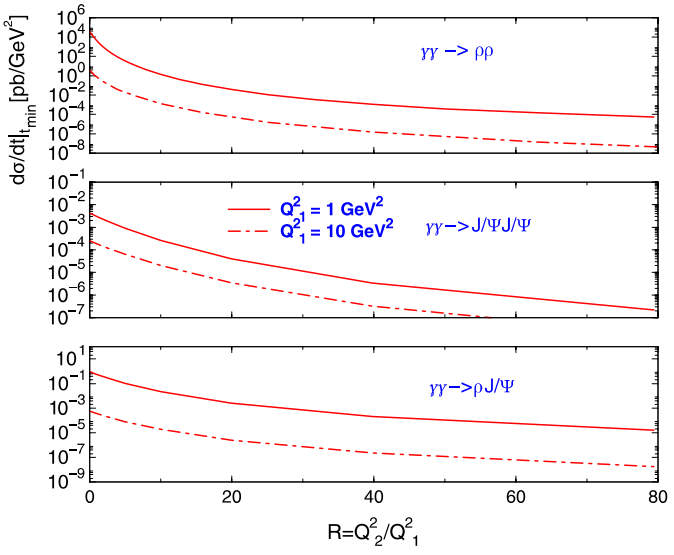

Fig. 7. Dependence of the forward differential cross section on the ratio $R = Q_2^2/Q_1^2$ of the photon virtualities at Q_1^2 fixed

Fig. 7 we present the dependence of the forward differential cross section on the ratio $R = Q_2^2/Q_1^2$ at fixed Q_1^2. We consider the typical values $Q_1^2 = 1$ and $Q_1^2 = 10\,\mathrm{GeV}^2$. In all cases, the cross section decreases as Q_2^2 increases, presenting finite values towards $R = 0$. It should mentioned that this interpolation can not be obtained in the BFKL approach in view of the lack of a scale in the process. In our case, the saturation scale provides the semi-hard scale. In order to investigate the quantitative behavior on R at intermediate virtualities, we adjust the curves with the simple exponential parameterization for $R \geq 1$ in the form $\left.\frac{\mathrm{d}\sigma_{V_1V_2}}{\mathrm{d}t}\right|_{t_\mathrm{min}=0} \propto \mathrm{e}^{-\beta R}$. This procedure gives $\beta = 4.4$, 2.6, 2.9 for double ϱ, double J/Ψ and $\varrho J/\Psi$, respectively. The

results follow the typical saddle-point BFKL solution in the region of $R \geq 5\,\mathrm{GeV}^2$, namely the cross sections behave as $\frac{\mathrm{d}\sigma_{V_1V_2}}{\mathrm{d}t}\Big|_{t_{\min}=0} \propto \frac{1}{Q_1^2Q_2^2}\exp(-\beta \ln^2 R)$ as computed in [40]. It should be noticed that our definition for R is slightly different from that reference.

3.3 Investigating saturation effects

Let us now investigate the magnitude of saturation effects in the differential cross section comparing the results using the small $r_{\rm eff}$ approximation for the dipole–dipole cross section with the complete expression including the transition for the saturation regime (see discussion in Sect. 2.2). We restrict our analysis to a comparison between the linear and saturation model predictions for double ϱ and J/Ψ production. The results are shown in Fig. 8, where solid lines stand for the resummed calculations and dot-dashed one for the linear approximation. It should be noticed that the saturation scale is different for each meson because $Q^2_{\rm sat} \approx (x_0/x_{12})^{0.3}$ and x_{12} depends on the meson mass as defined in (1). For the most striking case, in the production by two real photons, the saturation scale for ϱ reaches $Q^2_{\rm sat} \approx 2.5\,\mathrm{GeV}^2$ whereas it stays as $Q^2_{\rm sat} \approx 1\,\mathrm{GeV}^2$ for J/Ψ. Therefore, the saturation scale is higher for ϱ than for J/Ψ up to intermediate virtualities. Let us start discussing double J/Ψ production (see Fig. 8b), which is one typical hard process characterized by a hard scale given by $\mu^2(Q, M_V) = 2(Q^2 + M^2_{J/\Psi})$. Consequently, we may expect a perturbative description to be valid even in the real photon limit, $Q^2 \to 0$, and that the contribution from the saturation effects to be small while $\mu^2 \gg Q^2_{\rm sat}$. However, as the saturation scale grows with the energy, the saturation effects become important at large energies. This is the reason we observe a difference between linear and resummed predictions at $W \approx 1$ TeV in the real photon case. These results indicate that double J/Ψ production is not strongly modified by saturation corrections for energies smaller than 1 TeV. On the other hand, in double ϱ production the situation changes drastically. For real photons, it is a typical soft process and, therefore, in this case the linear and saturation predictions are very distinct. Now, the scale is given by $\mu^2(Q, M_V) = 2(Q^2 + M^2_\varrho)$, which should be treated carefully due to the small meson mass. The results are presented in Fig. 8a. In the real photon scattering, one has $\mu^2 = 2M^2_\varrho \approx 1\,\mathrm{GeV}^2$ and therefore saturation effects are increasingly important as $\mu^2 < Q^2_{\rm sat}(W_{\gamma\gamma})$, which explains the reason for the cross section to be reduced by two orders of magnitude at $W_{\gamma\gamma} \simeq 1$ TeV. At $Q^2 = 10\,\mathrm{GeV}^2$, the scenario is different since $\mu^2 = 2Q^2 \geq Q^2_{\rm sat}$. Therefore, the resummed prediction is similar to the linear one, but corrections for large energies are still important. In view of the discussions above, double ϱ production becomes an ideal place to probe the saturation physics.

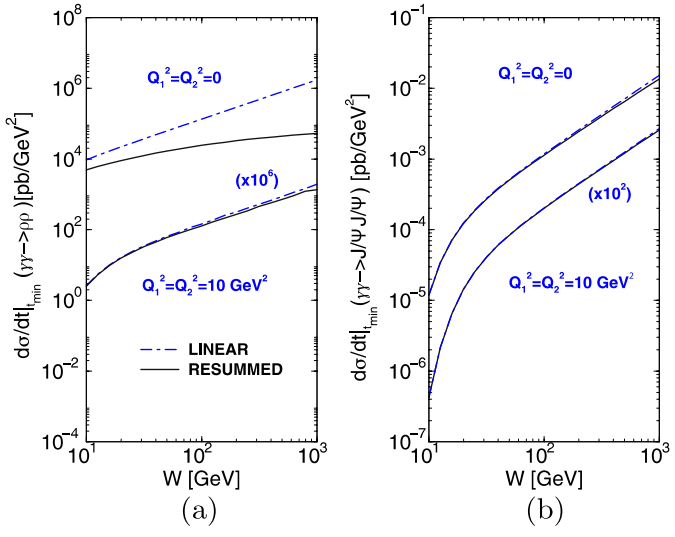

Fig. 8. Comparison between the linear and saturation predictions for the energy dependence of the forward differential cross section: **a** double ϱ production and **b** double J/Ψ production

4 Summary

In this paper we have extended the dipole picture for double vector meson production, $\gamma^*(Q_1)\gamma^*(Q_2) \to V_1V_2$, and we have calculated the forward differential cross section assuming that the dipole–dipole cross section can be modeled by a saturation model. We have analyzed the energy and virtuality dependence and investigated the magnitude of saturation effects. It is found that the effective power of the energy is directly dependent on the typical momentum scale for the process, $\mu^2 = Q_1^2 + Q_2^2 + M^2_{V_1} + M^2_{V_2}$, which is different for distinct meson pair and photon virtualities. Saturation effects are important for double ϱ production on real photons, whereas is small for processes containing J/Ψ and/or large photon virtualities. It is shown the contribution of the distinct polarizations and their regions of dominance for each meson pair. The results are consistent with expectations from electroproduction of vector mesons. The dependence on virtuality has been investigated using the analysis on the ratio $R = Q_2^2/Q_1^2$. The results are qualitatively in agreement with previous predictions obtained using the dipole or NLO BFKL approaches. Our results demonstrate that double meson production in two-photon interactions at high energies offer an ideal opportunity for the study of the transition between the linear and saturation regimes.

Acknowledgements. VPG would like to thanks W.K. Sauter for informative and helpful discussions. MM thanks for the support of the High Energy Physics Phenomenology Group, GFPAE IF-UFRGS, Brazil. The authors are grateful to C. Marquet for his valuable comments and suggestions. This work was partially financed by the Brazilian funding agencies CNPq and FAPERGS.

References

1. L.N. Lipatov, Sov. J. Nucl. Phys. **23**, 338 (1976)
2. E.A. Kuraev, L.N. Lipatov, V.S. Fadin, JETP **45**, 1999 (1977)
3. I.I. Balitskii, L.N. Lipatov, Sov. J. Nucl. Phys. **28**, 822 (1978)

4. V.N. Gribov, L.N. Lipatov, Sov. J. Nucl. Phys. **15**, 438 (1972)
5. G. Altarelli, G. Parisi, Nucl. Phys. B **126**, 298 (1977)
6. Y.L. Dokshitzer, Sov. Phys. JETP **46**, 641 (1977)
7. I. Balitsky, Nucl. Phys. B **463**, 99 (1996)
8. Y.V. Kovchegov, Phys. Rev. D **60**, 034008 (1999)
9. Y.V. Kovchegov, Phys. Rev. D **61**, 074018 (2000)
10. L.D. McLerran, R. Venugopalan, Phys. Rev. D **49**, 2233 (1994)
11. E. Iancu, A. Leonidov, L. McLerran, Nucl. Phys. A **692**, 583 (2001)
12. E. Ferreiro, E. Iancu, A. Leonidov, L. McLerran, Nucl. Phys. A **703**, 489 (2002)
13. J. Jalilian-Marian, A. Kovner, L. McLerran, H. Weigert, Phys. Rev. D **55**, 5414 (1997)
14. J. Jalilian-Marian, A. Kovner, H. Weigert, Phys. Rev. D **59**, 014014 (1999)
15. J. Jalilian-Marian, A. Kovner, H. Weigert, Phys. Rev. D **59**, 014015 (1999)
16. J. Jalilian-Marian, A. Kovner, H. Weigert, Phys. Rev. D **59**, 034007 (1999)
17. A. Kovner, J. Guilherme Milhano, H. Weigert, Phys. Rev. D **62**, 114005 (2000)
18. H. Weigert, Nucl. Phys. A **703**, 823 (2002)
19. K. Golec-Biernat, M. Wüsthoff, Phys. Rev. D **60**, 114023 (1999)
20. K. Golec-Biernat, M. Wüsthoff, Phys. Rev. D **59**, 014017 (1998)
21. J. Bartels, K. Golec-Biernat, H. Kowalski, Phys. Rev. D **66**, 014001 (2002)
22. H. Kowalski, D. Teaney, Phys. Rev. D **68**, 114005 (2003)
23. E. Iancu, K. Itakura, S. Munier, Phys. Lett. B **590**, 199 (2004)
24. N. Timneanu, J. Kwiecinski, L. Motyka, Eur. Phys. J. C **23**, 513 (2002)
25. N.N. Nikolaev, B.G. Zakharov, Z. Phys. C **49**, 607 (1991)
26. N.N. Nikolaev, B.G. Zakharov, Z. Phys. C **53**, 331 (1992)
27. A.H. Mueller, Nucl. Phys. B **415**, 373 (1994)
28. A.H. Mueller, B. Patel, Nucl. Phys. B **425**, 471 (1994)
29. N.N. Nikolaev, J. Speth, V.R. Zoller, Eur. Phys. J. C **22**, 637 (2002)
30. N.N. Nikolaev, J. Speth, V.R. Zoller, J. Exp. Theor. Phys. **93**, 957 (2001)
31. N.N. Nikolaev, J. Speth, V.R. Zoller, Zh. Eksp. Teor. Fiz. **93**, 1104 (2001)
32. A. Donnachie, H.G. Dosch, M. Rueter, Phys. Rev. D **59**, 074011 (1999)
33. J. Kwiecinski, L. Motyka, Phys. Lett. B **438**, 203 (1998)
34. J. Kwiecinski, L. Motyka, Acta Phys. Pol. B **30**, 1817 (1999)
35. L. Motyka, B. Ziaja, Eur. Phys. J. C **19**, 709 (2001)
36. V.P. Goncalves, M.V.T. Machado, Eur. Phys. J. C **28**, 71 (2003)
37. V.P. Goncalves, M.V.T. Machado, Eur. Phys. J. C **29**, 271 (2003)
38. V.P. Goncalves, W.K. Sauter, Eur. Phys. J. C **44**, 515 (2005)
39. B. Pire, L. Szymanowski, S. Wallon, Eur. Phys. J. C **44**, 545 (2005)
40. R. Enberg, B. Pire, L. Szymanowski, S. Wallon, Eur. Phys. J. C **45**, 759 (2006)
41. D.Y. Ivanov, A. Papa, Nucl. Phys. B **732**, 183 (2006)
42. V. Barone, E. Predazzi, High-Energy Particle Diffraction (Springer, Berlin Heidelberg, 2002)
43. S. Munier, A.M. Stasto, A.H. Mueller, Nucl. Phys. B **603**, 427 (2001)
44. J.R. Forshaw, R. Sandapen, G. Shaw, Phys. Rev. D **69**, 094013 (2004)
45. H.G. Dosch, T. Gousset, G. Kulzinger, H.J. Pirner, Phys. Rev. D **55**, 2602 (1997)
46. N.N. Nikolaev, Comments Nucl. Part. Phys. **21**, 41 (1992)
47. I.P. Ivanov, N.N. Nikolaev, A.A. Savin, hep-ph/0501034
48. V.P. Goncalves, M.V.T. Machado, Eur. Phys. J. C **38**, 319 (2004)
49. M. Wirbel, B. Stech, M. Bauer, Z. Phys. C **29**, 637 (1985)
50. S.J. Brodsky, G.P. Lepage, Phys. Rev. D **22**, 2157 (1980)
51. E. Levin, K. Tuchin, Nucl. Phys. B **573**, 833 (2000)
52. C. Marquet, R. Peschanski, Phys. Lett. B **587**, 201 (2004)
53. OPAL Collaboration, G. Abbiendi et al., Eur. Phys. J. C **14**, 199 (2000)
54. L3 Collaboration, M. Acciarri et al., Phys. Lett. B **519**, 33 (2001)
55. M.G. Ryskin, Z. Phys. C **57**, 89 (1993)